Proceedings of the Sixteenth International Conference on
Computational Structures Technology
Edited by: P. Iványi, J. Kruis and B.H.V. Topping
Civil-Comp Conferences, Volume 14, Paper 6.3
Civil-Comp Press, Edinburgh, United Kingdom, 2026
ISSN: 2753-3239, doi: 10.4203/ccc.14.6.3

Topology Optimization Design of Multimaterial Heterogeneous Interfaces for Additive Manufacturing

Z. Cai, L. Meng, D. Huo, J. Zhang, Y. Wang, J. Zhu and W. Zhang

State IJR Center of Aerospace Design and Additive Manufacturing, Northwestern Polytechnical University, Xi'an, China

Abstract

This paper presents a thermostructural topology optimization method for the design of multimaterial heterogeneous interfaces in additive manufacturing, where efficient heat transport and reliable load carrying must be achieved simultaneously. The spatial distribution of two constituent materials is employed as a unified design variable, and an optimization framework is established by coupling the steady-state heat conduction equation, the structural equilibrium equation, the thermal compliance objective, and the constraints on allowable stress and material volume fraction. A horizontally layered reference layout is adopted as the common initial configuration so that the interface evolution induced by different boundary conditions can be assessed on a consistent basis. Numerical investigations show that the proposed method generates continuous, stable, and physically interpretable heterogeneous interfaces under regular thermal and mechanical boundaries. The highly conductive phase preferentially reconstructs the dominant heat-flow path, whereas the high-allowable-stress phase is concentrated around the support and loading regions to preserve structural safety. Compared with the initial layered configuration, the optimized designs achieve a marked reduction in thermal compliance together with improved mean and peak temperature levels. The results confirm that the unified treatment of heat-transfer behavior, stress safety, and interface organization provides an effective foundation for the high-performance design of multimaterial structures for additive manufacturing.

Keywords: topology optimization, heterogeneous interface, additive manufacturing, thermal compliance, thermostructural design, multimaterial

1 Introduction

Additive manufacturing offers a level of geometric and material freedom that is difficult to achieve by conventional fabrication routes. For structures required to perform thermal management and mechanical load bearing at the same time, the key design issue is no longer the selection of a single material but the coordinated spatial arrangement of multiple functional materials. A highly conductive material promotes the establishment of efficient heat-transfer channels, whereas a material with a higher allowable stress is better suited to support concentrated loads and suppress local failure. Once these materials are integrated into the same component, the location, shape, and continuity of the interface become decisive for the overall performance [1, 2].

Multimaterial topology optimization provides a systematic framework for addressing this class of problems. Previous studies have shown that material interpolation, interface regulation, and multiphysics modeling can be combined to realize directional material placement within a common design domain and to alter both heat-flow paths and stress-transfer paths in a nontrivial manner [3, 4]. In thermal design, classical formulations usually minimize thermal compliance, thermal resistance, or peak temperature [5]. In structural design, the most common criteria involve compliance, displacement, or stress safety. The difficulty arises because thermal objectives generally favor the formation of continuous high-conductivity paths, whereas structural constraints favor the retention of mechanically stronger material along support and loading regions. As a consequence, multimaterial interface optimization is intrinsically governed by competing physical requirements.

From the standpoint of additive manufacturing, the geometry of the optimized interface also carries direct process implications. If the resulting material layout is excessively fragmented, discontinuous, or devoid of a dominant organization direction, an improved thermal metric alone does not necessarily translate into a manufacturable design [6, 7]. For this reason, it is more meaningful to study interface morphologies that emerge under regular boundary conditions and clear physical mechanisms than to focus on visually complex local optima produced under arbitrary settings. Such interfaces are easier to interpret, easier to compare, and more compatible with subsequent process mapping.

On this basis, the present study develops a thermostructural topology optimization framework for multimaterial heterogeneous interfaces under regular thermal and mechanical boundary conditions, with particular attention to additive manufacturing applications. Starting from a unified horizontally layered reference structure, the paper examines how the boundary conditions govern interface evolution. The main features of the present study are threefold. First, the distributions of the high-allowable-stress phase and the high-conductivity phase are treated as a single set of design variables so that thermal and mechanical design are handled in a coupled manner. Second, thermal compliance is adopted as the primary objective, while allowable stress and volume fraction constraints are imposed to preserve physical and structural plausibility. Third, representative cantilever and fixed-fixed beam examples are employed to show how regular boundary conditions promote clearly layered multimaterial interfaces and to clarify their implications for additive manufacturing.

2 Methodology

In this section we present the formulation used for the multimaterial thermostructural interface design problem.

2.1 Design Variables and Material Interpolation

Consider the two-dimensional rectangular design domain

$$\Omega = [0, L_x] \times [0, L_y] \subset \mathbb{R}^2, \tag{1}$$

where L_x and L_y denote the lengths of the domain in the x and y directions, respectively. The domain is discretized into N_e four-node quadrilateral elements. For each element e, a design variable $\rho_e \in [0, 1]$ is introduced. The value $\rho_e = 1$ indicates that the element is fully occupied by material A, which has a higher allowable stress, whereas $\rho_e = 0$ indicates that the element is fully occupied by material B, which has a higher thermal conductivity.

The material properties are interpolated linearly as

$$\begin{aligned} E(\rho_e) &= \rho_e E_A + (1 - \rho_e) E_B, \\ k(\rho_e) &= \rho_e k_A + (1 - \rho_e) k_B, \\ \sigma_{\text{allow}}(\rho_e) &= \rho_e \sigma_A + (1 - \rho_e) \sigma_B, \end{aligned} \tag{2}$$

where $E(\rho_e)$ is the effective Young's modulus of element e, $k(\rho_e)$ is the effective thermal conductivity, and $\sigma_{\text{allow}}(\rho_e)$ is the effective allowable stress. The constants E_A, k_A, and σ_A represent the Young's modulus, thermal conductivity, and allowable stress of material A, respectively, whereas E_B, k_B, and σ_B denote the corresponding parameters of material B.

2.2 State Equations and Boundary Conditions

For a prescribed material distribution $\boldsymbol{\rho} = [\rho_1, \rho_2, \ldots, \rho_{N_e}]^{\mathsf{T}}$, the steady-state temperature field $\boldsymbol{T}$ and the displacement field $\boldsymbol{u}$ are governed by

$$\boldsymbol{K}_T(\boldsymbol{\rho})\boldsymbol{T} = \boldsymbol{Q}, \tag{3}$$

$$\boldsymbol{K}_u(\boldsymbol{\rho})\boldsymbol{u} = \boldsymbol{f}, \tag{4}$$

where $\boldsymbol{K}_T(\boldsymbol{\rho})$ is the thermal conductivity matrix, $\boldsymbol{Q}$ is the thermal load vector, $\boldsymbol{K}_u(\boldsymbol{\rho})$ is the structural stiffness matrix, and $\boldsymbol{f}$ is the external load vector.

Two types of mechanical supports are considered. For the cantilever beam, the left boundary is fully clamped:

$$\Gamma_u^{\mathrm{C}} = \{(x, y) \in \partial\Omega \mid x = 0\}, \qquad \boldsymbol{u} = \boldsymbol{0} \text{ on } \Gamma_u^{\mathrm{C}}. \tag{5}$$

For the fixed-fixed beam, both end boundaries satisfy

$$\Gamma_u^{\mathrm{CC}} = \{x = 0\} \cup \{x = L_x\}, \qquad \boldsymbol{u} = \boldsymbol{0} \text{ on } \Gamma_u^{\mathrm{CC}}. \tag{6}$$

All retained examples in this paper employ the same thermal boundary pattern, namely a uniform heat-flux input on the top boundary and a prescribed temperature on the bottom boundary:

$$-k\nabla T \cdot \boldsymbol{n} = q_0 \text{ on } \Gamma_q = \{y = L_y\}, \qquad T = T_c \text{ on } \Gamma_T = \{y = 0\}, \tag{7}$$

where q_0 is the uniform heat-flux density applied on the top surface, T_c is the prescribed cooling temperature on the bottom surface, and $\boldsymbol{n}$ denotes the outward unit normal.

To ensure a consistent comparison across examples, all optimizations start from the same horizontally layered reference structure. If the prescribed upper limit of the volume fraction of material A is f_A, the initial design is defined as

$$\rho^{(0)}(x, y) = \begin{cases} 1, & y \geq L_y(1 - f_A), \\ 0, & y < L_y(1 - f_A), \end{cases} \tag{8}$$

which places a layer of material A in the upper portion of the design domain and a layer of material B in the lower portion. This choice provides a clear layered reference, making it possible to track how the optimized interface departs from the initial parallel layout.

2.3 Optimization Model

Under a prescribed thermal load $\boldsymbol{Q}$, the optimization objective is the thermal compliance

$$J_{\mathrm{th}}(\boldsymbol{\rho}) = \boldsymbol{Q}^{\mathsf{T}}\boldsymbol{T}. \tag{9}$$

Here, J_{th} measures the global thermal response associated with the imposed heat input. For a fixed thermal loading, a smaller thermal compliance generally corresponds to a more efficient conductive pathway and a lower overall thermal response.

To control local stress risk, an allowable-stress constraint is introduced in KS-aggregated form:

$$g_\sigma(\boldsymbol{\rho}) = \frac{1}{p_{\mathrm{KS}}} \ln \left[\sum_{e=1}^{N_e} \exp\left(p_{\mathrm{KS}} \left(\frac{\sigma_{\mathrm{vm},e}}{\sigma_{\mathrm{allow}}(\rho_e)} - 1 \right) \right) \right] \leq 0, \tag{10}$$

where $\sigma_{\mathrm{vm},e}$ is the von Mises stress of element e, $\sigma_{\mathrm{allow}}(\rho_e)$ is the local allowable stress, and p_{KS} is the KS aggregation parameter.

The total amount of material A is controlled by the volume-fraction constraint

$$g_V(\boldsymbol{\rho}) = \frac{1}{V}\sum_{e=1}^{N_e} v_e\rho_e - f_A \leq 0, \tag{11}$$

where v_e is the area of element e, $V = \sum_{e=1}^{N_e} v_e$ is the total area of the design domain, and f_A is the upper limit of the volume fraction of material A.

The multimaterial heterogeneous-interface topology optimization problem can then be written as

$$\begin{aligned} \min_{\boldsymbol{\rho}} \quad & J_{\mathrm{th}}(\boldsymbol{\rho}) \\ \text{s.t.} \quad & \boldsymbol{K}_T(\boldsymbol{\rho})\boldsymbol{T} = \boldsymbol{Q}, \\ & \boldsymbol{K}_u(\boldsymbol{\rho})\boldsymbol{u} = \boldsymbol{f}, \\ & g_\sigma(\boldsymbol{\rho}) \leq 0, \\ & g_V(\boldsymbol{\rho}) \leq 0, \\ & 0 \leq \rho_e \leq 1, \qquad e = 1, 2, \ldots, N_e. \end{aligned} \tag{12}$$

This formulation seeks an interface organization that remains structurally admissible while making the most effective use of a limited amount of the high-allowable-stress material.

2.4 Evaluation Indices

In addition to thermal compliance, the mean domain temperature and the maximum temperature are used to characterize the thermal performance. The mean temperature over the design domain is defined as

$$\bar{T}_\Omega = \frac{1}{|\Omega|}\int_\Omega T(\boldsymbol{x})\,\mathrm{d}\Omega, \tag{13}$$

where $|\Omega|$ is the area of the design domain and $T(\boldsymbol{x})$ is the temperature at position $\boldsymbol{x}$. The maximum temperature is defined as

$$T_{\max} = \max_{\boldsymbol{x}\in\Omega} T(\boldsymbol{x}). \tag{14}$$

To quantify the improvement in the objective, the reduction ratio of thermal compliance is defined as

$$\eta_J = \frac{J_{\mathrm{th}}^{(0)} - J_{\mathrm{th}}^{(\mathrm{opt})}}{J_{\mathrm{th}}^{(0)}} \times 100\%, \tag{15}$$

where $J_{\mathrm{th}}^{(0)}$ denotes the thermal compliance of the initial layered reference design and $J_{\mathrm{th}}^{(\mathrm{opt})}$ denotes that of the optimized design. All temperatures reported in this paper are given in °C.

3 Numerical Examples and Discussion

All examples share the same rectangular design domain with length $L_x = 3.0\,\mathrm{m}$, height $L_y = 0.3\,\mathrm{m}$, and structural thickness 0.02 m. The finite element mesh consists of 120×12 four-node quadrilateral elements. The properties of material A are taken as $E_A = 72\,\mathrm{GPa}$, $k_A = 60\,\mathrm{W/(m\,K)}$, and $\sigma_A = 600\,\mathrm{MPa}$, whereas those of material B are $E_B = 69\,\mathrm{GPa}$, $k_B = 240\,\mathrm{W/(m\,K)}$, and $\sigma_B = 180\,\mathrm{MPa}$. The upper limit of the volume fraction of material A is uniformly set to $f_A = 0.30$. The thermal boundary conditions are fixed at a uniform heat flux $q_0 = 1.0 \times 10^5\,\mathrm{W/m^2}$ on the top surface and a prescribed temperature $T_c = 0\,^\circ\mathrm{C}$ on the bottom surface. All examples start from the layered reference design so that the interface evolution under different boundary conditions can be compared directly.

3.1 Cantilever Beam under Through-Thickness Heating

The first example considers a cantilever beam. The left end is fully clamped, and a vertical point load $F_y = -8.0 \times 10^4\,\mathrm{N}$ is applied at the mid-height of the free end. Heat enters from the top surface and is conducted downward through the thickness. This example is intended to examine how an asymmetric support condition drives the material interface away from the initial parallel layering and how the conductive pathway competes with the load-transfer pathway.

The results are presented in Figure 1. Relative to the initial layered reference structure, the thermal compliance is reduced by 26.32 %, from 1.50×10^6 to 1.11×10^6. The mean domain temperature decreases from 86.54 °C to 84.14 °C, indicating an overall improvement in the thermal response. By contrast, the maximum temperature rises from 250.00 °C to 266.07 °C, which implies that a local hot spot remains near the free-end region. At the same time, the structural compliance decreases from 1.82×10^4 to 1.81×10^4, and the maximum normalized stress overrun index drops from 3.055 to 0.264, showing a substantial mitigation of stress concentration.

The optimized material layout reveals that material B, the high-conductivity phase, forms a continuous heat-transfer channel through the beam interior. Material A, the high-allowable-stress phase, is preferentially retained near the clamped end and along the mechanical load path. This distribution indicates that the cantilever condition causes the interface to bend markedly in the vicinity of the support so as to balance thermal transport efficiency against structural safety. Because the support condition is strongly asymmetric, the optimized interface no longer remains strictly parallel to the initial layered arrangement. Instead, it develops into an asymmetric layered pattern biased toward the fixed end. The result suggests that, under cantilever conditions, multimaterial interface optimization places greater emphasis on local load-bearing protection, and the benefit of optimization is reflected more clearly by the reduction in thermal compliance than by a reduction in the peak temperature.

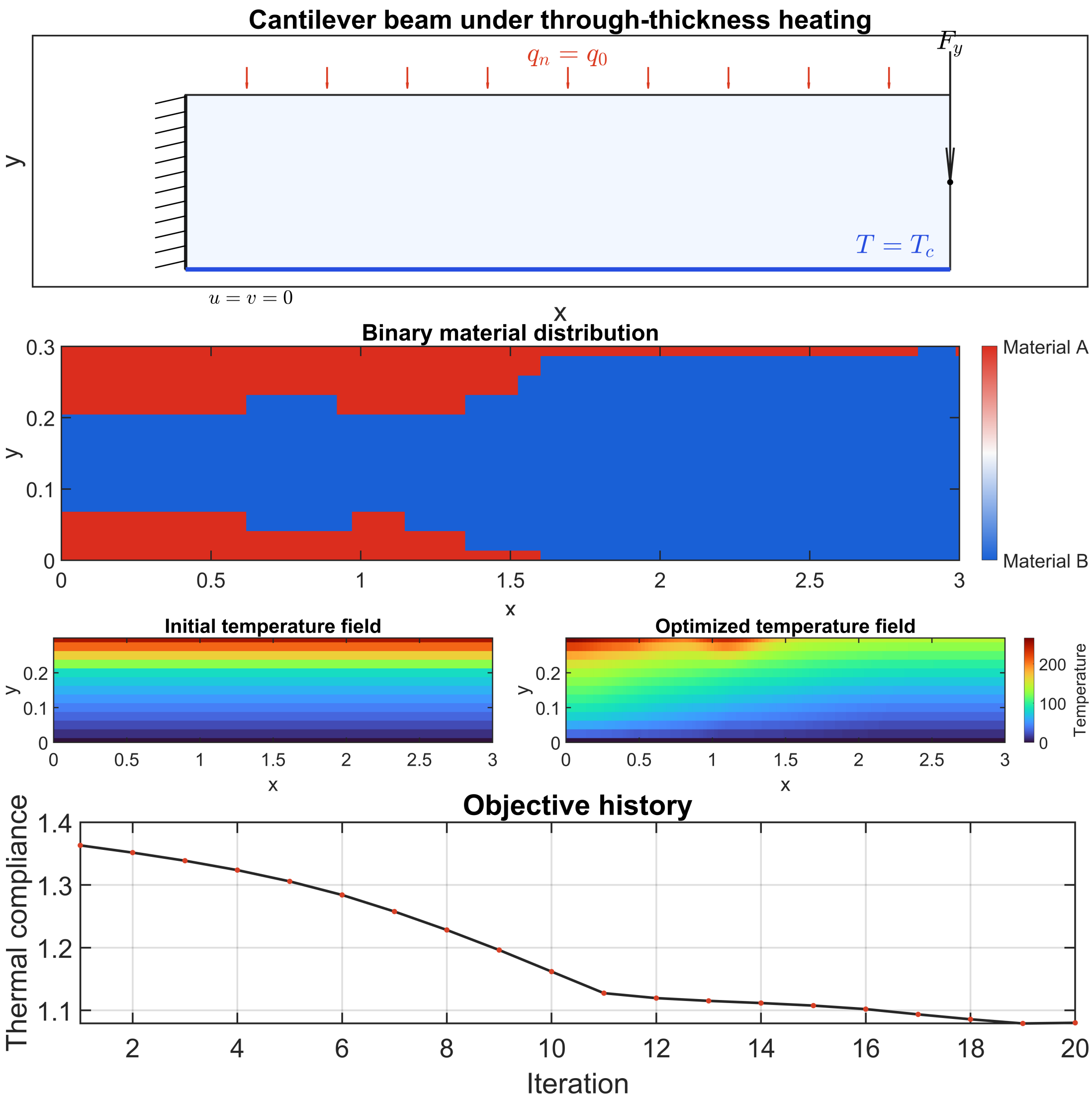

Figure 1: Optimization results for the cantilever beam subjected to through-thickness heating. The figure shows, in sequence, the boundary conditions, the optimized material distribution, the comparison between the initial and optimized temperature fields, and the iterative history of thermal compliance. A unified color scale is used for the temperature comparison.

3.2 Fixed-Fixed Beam under Through-Thickness Heating

The second example is a fixed-fixed beam. Both ends are fully clamped. A vertical point load $F_y = -8.0 \times 10^4\,\mathrm{N}$ is applied at the geometric center. The thermal boundary conditions remain a uniform heat flux on the top boundary and a prescribed temperature on the bottom boundary. Compared with the cantilever case, the mechanical support and the geometry are much more symmetric, making this example more suitable for observing layered interface organization under regular heat-flow and load-transfer conditions.

The results are shown in Figure 2. The thermal compliance is reduced by 49.34 %, from 1.50×10^6 to 7.60×10^5. The mean domain temperature drops from 86.54 °C to 62.84 °C. The maximum temperature decreases from 250.00 °C to 126.66 °C. These changes indicate a pronounced reduction in both the overall temperature level and the local peak temperature. The structural compliance increases only slightly, from 321.40 to 327.26. Meanwhile, the maximum normalized stress overrun index remains negative throughout the process, changing from -0.475 to -0.471. This confirms that the design stays on the safe side of the allowable-stress constraint during optimization.

Compared with the cantilever case, the fixed-fixed boundary condition suppresses global bending much more effectively and allows the interface to respond more directly to the thermal transport requirement. The optimized material distribution exhibits a clear and stable layered organization through the thickness: material A is mainly retained in the upper load-carrying layer and in local regions of force-flow concentration, while material B forms a continuous conductive layer in the lower part of the domain. Because the directions of heat input and cooling are well defined through the thickness, the optimized interface remains broadly consistent with the initial parallel layering and undergoes only localized adjustments around the central loading region. This result indicates that, under regular and nearly symmetric boundary conditions, multimaterial heterogeneous interfaces are more likely to evolve into layered patterns that are simultaneously thermally efficient, mechanically rational, and favorable for additive manufacturing.

3.3 Discussion

The two representative examples clarify the decisive role of boundary conditions in the formation of multimaterial heterogeneous interfaces. In the cantilever beam, the load path is strongly asymmetric between the fixed end and the free end, and the interface consequently evolves by locally thickening the mechanically stronger phase while simultaneously opening a conductive pathway for heat transfer. In the fixed-fixed beam, the boundary conditions are more regular and the global stiffness is higher, so the interface tends to preserve a straighter and more continuous layered arrangement, with only local corrections near the center. Although the morphologies differ, both examples follow the same design logic: the high-allowable-stress material is placed where the load-transfer path demands protection, whereas the high-conductivity material is placed where the dominant heat-flow path must be reinforced. The heterogeneous interface emerges as the result of balancing these two physical requirements.

From the perspective of additive manufacturing, the optimized layouts obtained in this study do not degenerate into scattered material patches. Instead, they form continuous layered organizations with a clear dominant direction. Such interface morphologies are better aligned with layerwise fabrication logic, easier to interpret in terms of process planning, and more likely to support subsequent toolpath or process-parameter mapping. The present framework therefore provides not only thermal and

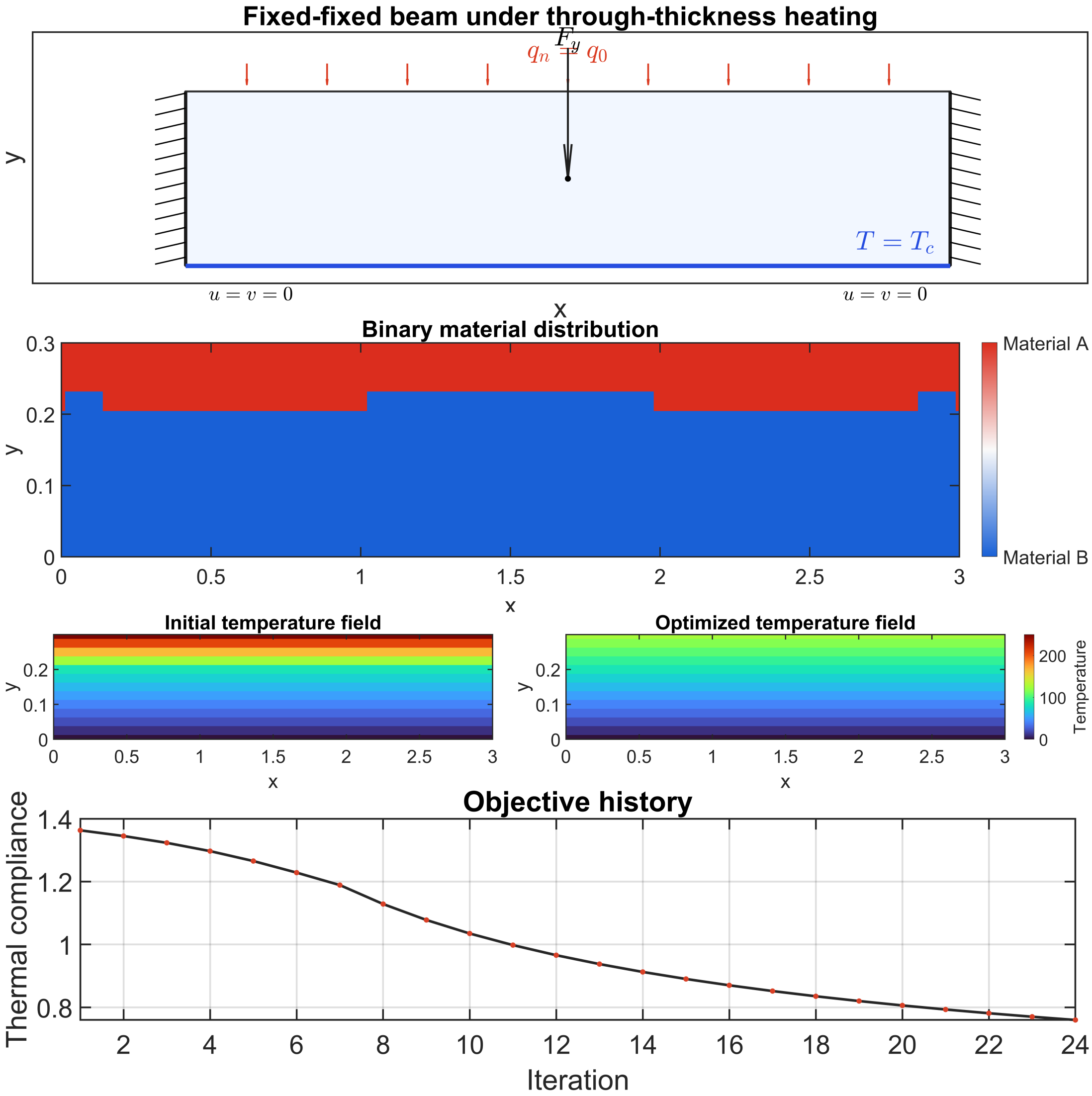

Figure 2: Optimization results for the fixed-fixed beam subjected to through-thickness heating. The figure shows, in sequence, the boundary conditions, the optimized material distribution, the comparison between the initial and optimized temperature fields, and the iterative history of thermal compliance.

structural improvement, but also a physically meaningful basis for designing multi-material interfaces in additively manufactured components.

4 Concluding Remarks

This work has developed a topology optimization method for multimaterial heterogeneous interfaces in additive manufacturing. By adopting the distribution of two constituent materials as the unified design variable, the method combines heat conduction analysis, structural analysis, thermal compliance minimization, allowable-stress control, and material volume-fraction limitation within a single framework. A common horizontally layered reference configuration is used as the initial design for all examples, making it possible to compare interface evolution under different boundary conditions on a consistent basis. Within this formulation, the interface is not treated as a secondary outcome of optimization, but as the central design object through which thermal transport and load-bearing requirements are reconciled.

The numerical results show that the proposed method generates continuous, interpretable, and distinctly layered multimaterial interfaces under regular thermal and mechanical boundary conditions. The high-conductivity material reconstructs the dominant heat-transfer path, whereas the high-allowable-stress material protects the support region and the load-bearing region. In this way, the optimized designs achieve a coordinated improvement in thermal response and structural safety. When the boundary conditions are regular and nearly symmetric, the resulting interface is particularly prone to develop into a stable layered configuration, a feature that is naturally compatible with the layerwise logic of additive manufacturing.

Overall, the study demonstrates that the concurrent treatment of thermal performance, mechanical safety, and interface organization in a unified topology optimization framework provides an effective route for the high-performance design of multi-material additively manufactured structures. The framework can be extended in future work to more complex geometries, a larger number of material phases, and more strongly coupled multiphysics problems.

Acknowledgements

The authors gratefully acknowledge the support provided by the State IJR Center of Aerospace Design and Additive Manufacturing, Northwestern Polytechnical University.

References

[1] J. Park, A. Sutradhar, A multi-resolution method for 3D multi-material topology optimization, Computer Methods in Applied Mechanics and Engineering, 285, 571–586, 2015.

[2] O. Giraldo-Londono, L. Mirabella, L. Dalloro, G.H. Paulino, Multi-material thermomechanical topology optimization with applications to additive manu-

facturing: Design of main composite part and its support structure, Computer Methods in Applied Mechanics and Engineering, 363, 112812, 2020.

[3] S. Chu, M. Xiao, L. Gao, H. Li, J. Zhang, X. Zhang, Topology optimization of multi-material structures with graded interfaces, Computer Methods in Applied Mechanics and Engineering, 346, 1096–1117, 2019.

[4] P. Liu, L. Shi, Z. Kang, Multi-material structural topology optimization considering material interfacial stress constraints, Computer Methods in Applied Mechanics and Engineering, 363, 112887, 2020.

[5] Q. Li, G.P. Steven, Y.M. Xie, O.M. Querin, Evolutionary topology optimization for temperature reduction of heat conducting fields, International Journal of Heat and Mass Transfer, 47(23), 5071–5083, 2004.

[6] S.L. Vatanabe, T.N. Lippi, C.R. de Lima, G.H. Paulino, E.C.N. Silva, Topology optimization with manufacturing constraints: A unified projection-based approach, Advances in Engineering Software, 100, 97–112, 2016.

[7] X. Guo, J. Zhou, W. Zhang, Z. Du, C. Liu, Y. Liu, Level set-based topology optimization with overhang constraint: Towards support-free additive manufacturing, Computer Methods in Applied Mechanics and Engineering, 339, 591–614, 2018.